

International Conference on Space Optics—ICSO 2022

Dubrovnik, Croatia

3–7 October 2022

Edited by Kyriaki Minoglou, Nikos Karafolas, and Bruno Cugny,



Molecular contamination testing with continuous-wave laser radiation at 1064 nm: de-risking activity for the LISA space mission



Molecular contamination testing with continuous-wave laser radiation at 1064 nm: de-risking activity for the LISA space mission

Nils Bartels^{*a}, Franz Hadinger^a, Gabriele Taube^a, Wolfgang Riede^a, Christian Dahl^b, Kai-Cristian Voss^b, Alessandra Ciapponi^c, Ricardo Martins^c, Linda Mondin^c

^aDeutsches Zentrum für Luft- und Raumfahrt (DLR), Institut für Technische Physik, Pfaffenwaldring 38-40, 70569 Stuttgart, Germany; ^bSpaceTech GmbH, Seelbachstr. 13, 88090 Immenstaad, Germany; ^cEuropean Space Agency (ESA), ESTEC, Keplerlaan 1, NL-2200 AG Noordwijk, The Netherlands

ABSTRACT

We investigate effects of laser-induced contamination (LIC) with contaminant materials and laser parameters relevant for the LISA space mission. To accelerate outgassing and a possible deposit formation, the contaminant materials have been heated to a temperature of up to 100 °C (nominal operating temperature of 20° C), and LIC tests were performed with a laser power density of up to 300 W/cm² (to be compared with expected 125 W/cm²). Neither in-situ measurements (laser transmission, polarization and wavefront), nor a careful microscopic inspection of the optical surfaces after the LIC tests showed indications of a laser-induced deposit formation. Condensation on optical surfaces could be observed. This is cautiously encouraging for LISA and indicates that the LIC concern may be reduced compared to what observed at shorter wavelength or with pulsed laser radiation.

Keywords: Laser-induced contamination, LIDAR, outgassing, gravitational wave, space laser, space qualification

1. INTRODUCTION

The Laser Interferometer Space Antenna (LISA) will be the first space based gravitational wave observatory and aims at providing access to the measurement of gravitational waves in the 0.1mHz to 1Hz frequency band. This range of frequencies can only be accessed from space (seismic noise limitations) and will detect gravitational waves from many sources, including compact objects captured by supermassive black holes (see Fig. 1). With an expected launch in the mid to late-2030s, LISA will consist of three widely spaced spacecrafts separated by 2.5 million km. In order to detect gravitational waves, continuous-wave (cw), 1064 nm laser beams propagating between the spacecrafts will be used to measure their distances with picometer accuracy. This high accuracy is achieved via time-delay interferometry, in which one link measurements (in total there are 6 one link measurements between the three spacecrafts) will be recombined with appropriate delays to form three (non-independent) Michelson interferometers.

One of many challenges for LISA is that the operation of lasers comes with the risk of generating Laser Induced Contamination (LIC), meaning the formation of deposits generated from the interaction of the laser radiation with molecular or particulate contamination and the optical surfaces.

In this publication, we first introduce the topic of LIC in space lasers and explain why LIC is a critical topic for the LISA space mission. We then describe the results of an initial laboratory test campaign in which we test for a possible deposit formation with a material mixture and laser parameters relevant for the LISA space mission.

*nils.bartels@dlr.de; phone +49 711 68628244; dlr.de

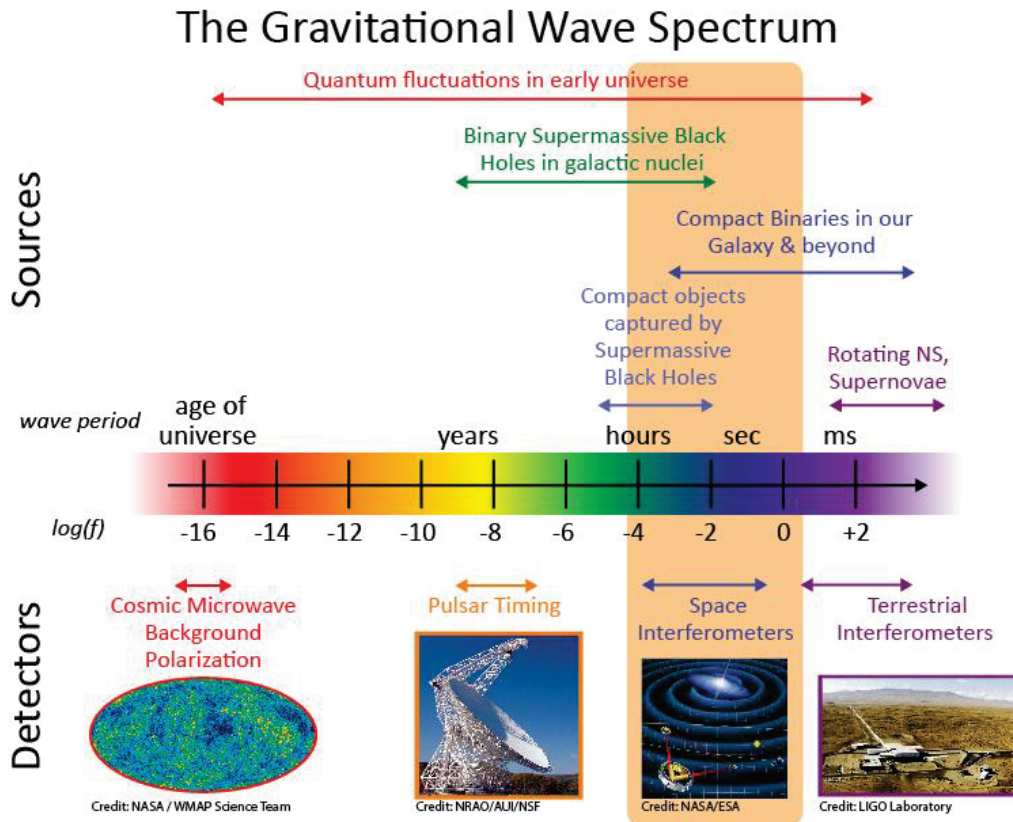


Figure 1: Sources of gravitational waves and detectors as function of the gravitational wave period. Credit: NASA Goddard Space Flight Center [1].

2. LASER-INDUCED CONTAMINATION AND ITS CRITICALITY FOR THE LISA MISSION

2.1 Laser-induced contamination in space lasers

LIC has been a critical conundrum for several space missions. In particular, the ESA mission Aeolus for measuring global wind profiles with a wind LIDAR using nanosecond-pulsed laser radiation at 355 nm, has only become possible after extensive ground-based test campaigns to find suitable materials. Furthermore, the laser head had to be redesigned for operating in a partial oxygen atmosphere instead of in vacuum [2, 3, 4]. LIC has also been proposed to be a contributor to severe performance losses on the LITE instrument and the GLAS laser on Icesat [5].

LIC is known to be particularly prominent for lasers operating in the ultraviolet (with a high photon energy that allows for bond breaking) and for short laser pulses (which trigger multi-photon absorption). The LISA space mission uses lasers with a wavelength of 1064 nm and continuous wave laser radiation, which significantly reduces the risk of LIC.

On the other hand, the LISA space mission can be expected to be sensitive even to very thin deposits affecting the wave front, consequently degrading gravitational wave detection performance. This will be explained in the following subsection. Furthermore, LISA targets a long mission duration (4.5 years with a planned extension of six years) and cumulative long-term effects need to be studied carefully to minimize their impact for this flagship mission.

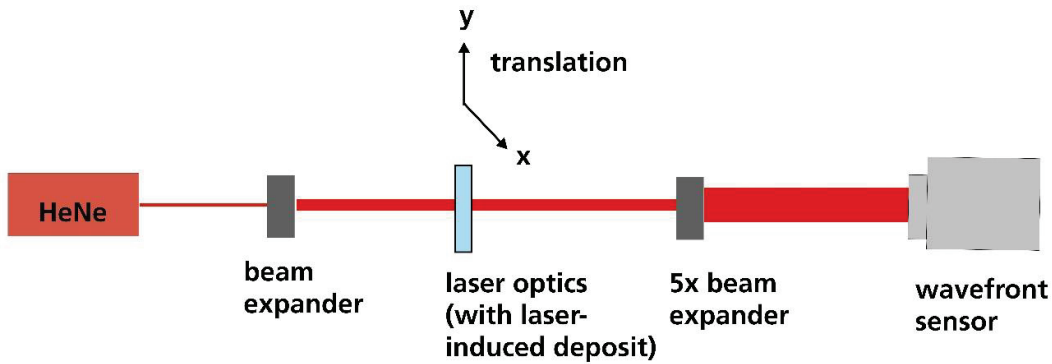
2.2 Why LIC is critical for the LISA space mission

For any laser-system, LIC can lead to a loss of performance or failure. In particular, a deposit on a laser optic can absorb laser-radiation. Transmission or reflection loss aside, the absorption of energy can also trigger laser-induced damage [6, 7]. An effect that has not been of concern for most missions so far, is that a laser-induced deposit induces minute changes to the laser-wavefront.

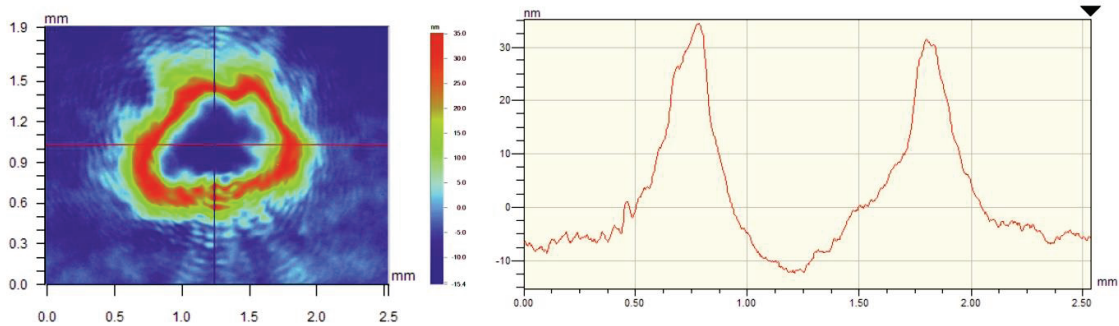
This effect has been showcased in a simple laboratory experiment, at DLR premises. We have measured the change of the wavefront of a Helium-Neon laser when passing through an optical component bearing a laser-induced deposit, see Figure 2. The deposit on the laser-optic had been generated in a previous LIC test with a nano-second pulsed laser at 266 nm [8]. The deposit (on the front side of the optics) had a height of ~40 nm with the typical “donut”-shape [8]. A similar shape was observed in the wavefront measurement of the Helium-Neon laser beam transmitted through the deposit. This effect relates to the change in the optical path length of the laser radiation transmitted at the location of the deposit.

The LISA mission has very high demands on the laser wavefront quality, in order to achieve interferometric distance measurements with picometer accuracy as required for the gravitational wave detection. The reasons are twofold, Firstly, the wavefront variations coupled with a S/C pointing jitter will create path length variations. Additionally, wavefront modifications will generate more scattering and loss of transmitted power to the distant S/C with a corresponding increase of the shot noise limit. The first -most important- effect was simulated mathematically and reported in literature [10, 11], and is qualitatively explained in Figure 3. In panel A of Figure 3, a laser is emitted from spacecraft 1 (SC 1) and forms a spherical wavefront (centered around SC 1) when reaching spacecraft 2 (SC 2), at a target distance of 2.5 million km. In this case, a small pointing jitter (a requirement for the LISA mission is $8 \times 10^{-9} \text{ rad Hz}^{-1/2}$) will not affect the measured distance. As opposed to this, a distorted wavefront will lead to an apparent distance that changes with the attitude of SC1 (see panel B of Figure 3). The LISA contamination working group has estimated that wavefront deformation of order of 2 nm per optical surface would start adversely affecting the gravitational waves detection performances. Of course, such small wavefront change could easily be introduced even by a very thin (nm level) laser-induced deposit.

A) Experimental setup:



B) Deposit morphology (WLIM) of laser optics:



C) Measured wavefront:

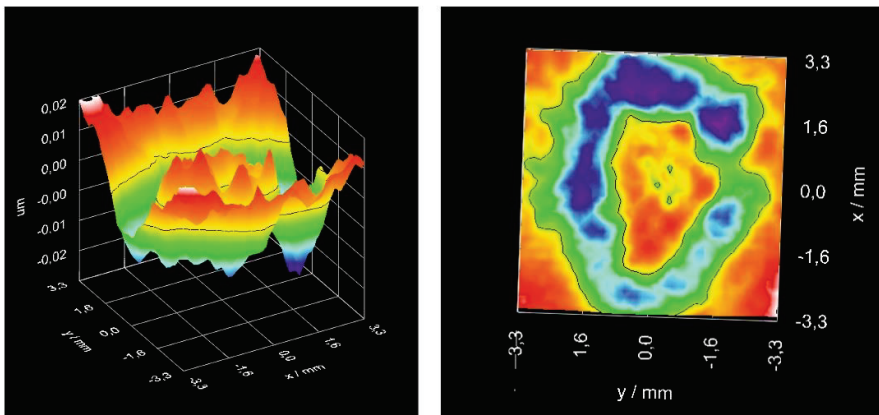


Figure 2: Wavefront changes induced by a laser-induced deposit. A) Experimental setup for detecting the laser-induced wavefront. B) Deposit morphology as measured with white-light interference microscopy (WLIM). C) Wavefront detected at the Shack-Hartmann wavefront sensor.

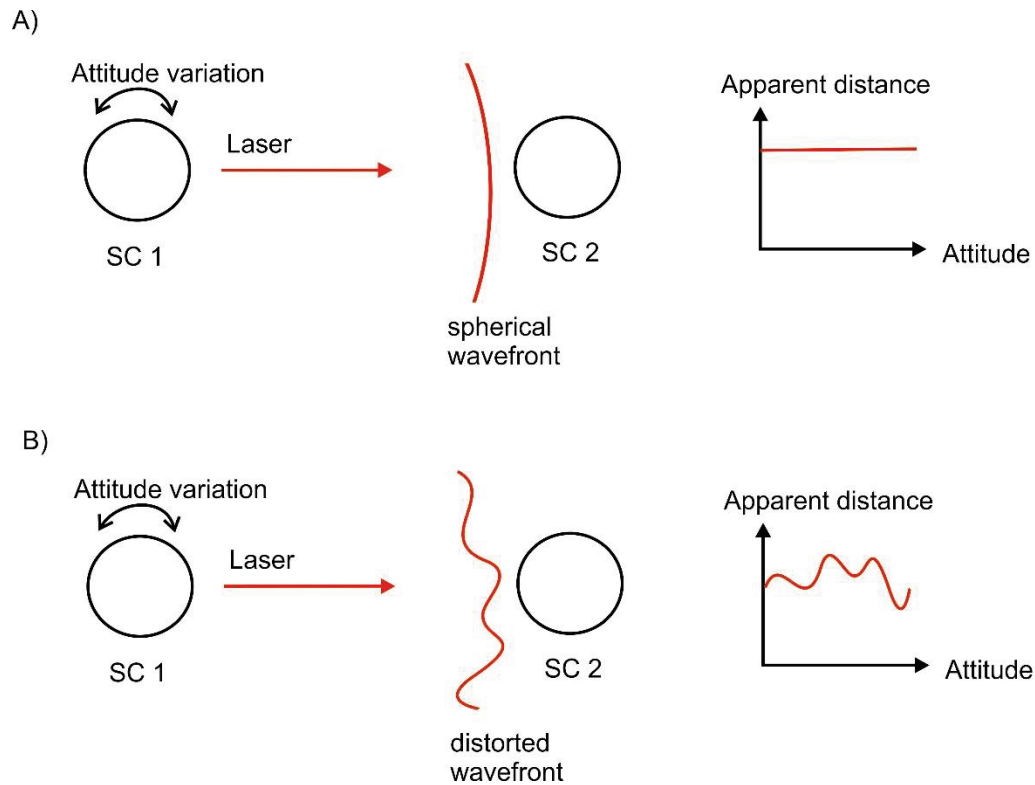


Figure 3: Explanation for the coupling of the wavefront to the jitter (attitude variation) of spacecraft 1 (SC 1) to the apparent distance measured at spacecraft 2 (SC 2) for a spherical wavefront centered around SC1 (panel A) and a distorted wavefront (panel B). The distorted wavefront will introduce a strong dependence of the distance measured between the spacecrafts on the attitude of SC1 (pointing jitter). Such a wavefront distortion can for example be introduced by a laser-induced deposit.

3. EXPERIMENTAL

3.1 Experimental setup

Figure 4 shows a schematic of the experimental setup used for LIC testing. The main part is a vacuum chamber composed of standard CF components with copper sealings, a chamber volume of ~30 liters and a base pressure of $<10^{-8}$ mbar obtained with using a turbo-molecular pump backed by a scroll pump.

The sample holder made from stainless steel is located in the centre of the LIC chamber and has one position for mounting a high-reflective sample (~20 degrees angle of incidence) and one position for mounting an anti-reflective sample (0° angle of incidence), see Figure 5. Additionally, a CaF_2 witness sample (Korth Kristalle GmbH) for contamination control via Fourier-transform infrared (FT-IR) spectroscopy [12] is mounted to a third position. The temperature of the sample holder can be monitored with a thermocouple and a thermal button logger (tempmate.®-B5). The sample holder can be translated along the z-direction with a high-resolution linear actuator (Physikalische Instrumente GmbH, M-230.25).

Molecular contamination is introduced by a contamination source, which is made from copper and designed as an effusion cell with three holes of 10 mm diameter. For LIC testing, we used a distance of ~35 mm between the holes of the effusion cell and the laser optics. The source was heated via heating cartridges and the temperature was monitored with a thermocouple. A heat shield made from stainless steel reduced the radiative heat transfer from the source to the sample

holder. By additionally wrapping parts of the contamination source with Aluminium foil (without covering the emission holes), it was possible to heat the contaminant up to 120°C, while keeping the sample holder at temperatures between 20°C and 25°C.

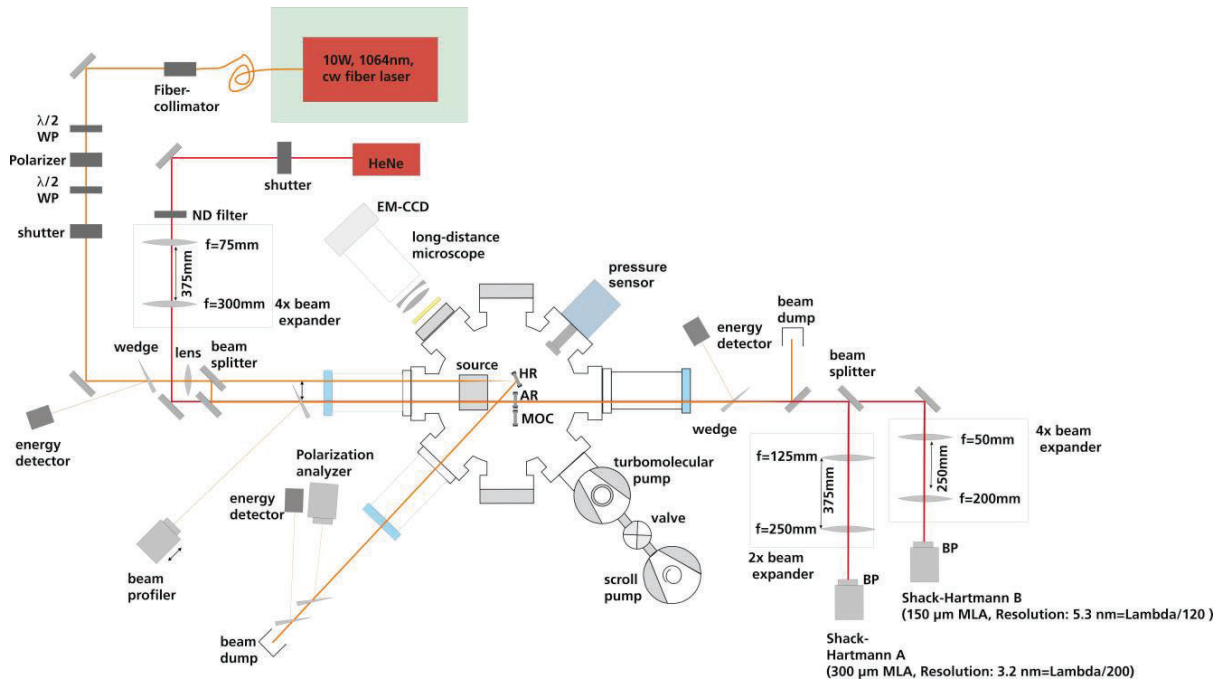


Figure 4: LIC Setup for LISA contamination testing. EM-CCD = electron-multiplying CCD camera, WP=wave plate, HR = high-reflection coated optics, AR=anti-reflection coated optics, MOC=CaF₂ witness sample.

For LIC testing, the optics under test were irradiated with a continuous-wave, 1064 nm fibre laser (IPG Photonics Inc., YLR-10-1064-LP). The output of that laser was split into two beams to simultaneously irradiate the AR optics and the HR optics under test.

We used several in-situ measurements for detecting a possible deposit formation during the LIC test. In particular, the transmission of the AR optics and the reflection of the HR optics were measured with power detectors (Ophir PD300) probing reflections of the laser beam from fused silica wedges (see Figure 4). Furthermore, we measured the polarization of light reflected from the HR optics with a polarimeter (Thorlabs Inc. PAX1000IR1). Finally, we measured changes to the wavefront of a frequency stabilized HeNe laser (Spectra Physics 117A, 633 nm wavelength) that was spatially overlapped with the beam of the 1064 nm fiber laser. The spatial overlap of the two lasers on the front surface of the AR optics was controlled by detecting scattered light with a long-distance microscope and an electron-multiplying CCD camera. The reason for detecting the wavefront of an overlapped HeNe laser, instead of directly detecting the wavefront of the 1064 nm laser, was that wavefront measurements with the HeNe laser and our Shack-Hartmann wavefront sensors (WFS30, Thorlabs Inc.) were more repeatable and had a lower RMS measurement error. We used two Shack-Hartmann sensors (WFS30, Thorlabs Inc.) for wavefront detection, since there is a fundamental trade-off between wavefront resolution and wavefront lateral resolution in wavefront measurements with a Shack-Hartmann (SH) sensor [13]. The beam directed to the first SH-sensor (SH-A) was used with a 2x beam expansion and a 300 μm pixel pitch micro-lens array (MLA) with a specified resolution of 3.2 nm ($\lambda/200$). The second SH-sensor (SH-B) was used with a 4x beam expansion and uses a 150 μm pixel pitch MLA (with a specified resolution of 3.6 nm ($\lambda/100$)) to detect wavefront changes with

small lateral dimension. Note that the He-Ne laser was not maintained on during most of the testing (as this too could have been a source of LIC) but only at short intervals to obtain the wavefront measurement.

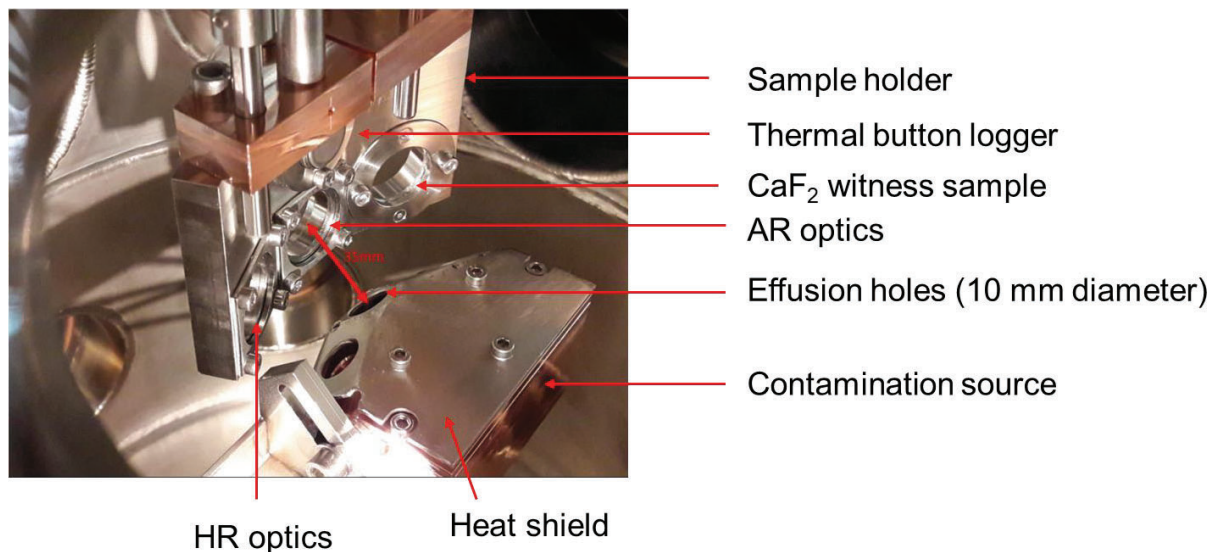


Figure 5: Contamination source and optics under test.

3.2 Tested materials and laser optics

Table 1 provides a list of contamination materials selected for the LIC test campaign. All materials (~1g each) were cured at room temperature (curing duration >7 days) on UHV compatible Aluminum foil. Afterwards, these materials were cut into small pieces to improve their homogeneity in the contamination source. Materials have been selected either because they were found to generate laser-induced deposits in previous LIC tests with nanosecond pulsed laser irradiation at 1064 nm [14] or because their usage is planned for the LISA mission.

The AR optics used for the LIC tests were electron-beam anti-reflection coated (AR/AR1064+532 @0° AOI), 1-inch diameter windows (fused silica substrate: PW1004UV, Laser Components GmbH) and were tested at an angle of incidence (AOI) of 0°. The HR optics used for the LIC tests were electron-beam high-reflection coated (HR 750 - 1100 nm @ 0-45°), 1-inch diameter mirrors (fused silica substrate: PW1004UV, Thorlabs Inc.) tested at an AOI of 22.5°.

Table 1. List of tested contamination materials.

Material	Description	Rationale
EC2216 (3M™ Scotch-Weld™ Epoxy Adhesive EC-2216 B/A)	Epoxy adhesive	Usage planned, deposit in IR pulsed LIC tests
NUSIL CV-2946 (Avantor Inc.)	Thermally conductive silicone	Usage planned
HYSOL Loctite EA9461 (Henkel AG)	Epoxy adhesive	Usage planned
Solithane C 113-300 (Uniroyal Chemical Company Inc.)	Polyurethane	Deposit in IR pulsed LIC tests
EPO-Tek 301-2 (Epoxy Technology Inc.)	Epoxy adhesive	Usage planned

3.3 Test procedure

LIC tests have been performed following the ISO technical report ISO/TR 20811 [12]. In particular, the laser optics were inspected before and after LIC testing via differential interference contrast (DIC) and fluorescence microscopy. Deviating from the ISO technical report, we have not used in-situ fluorescence detection, as presence thereof, at the LISA wavelength, is not expected to occur. Instead, in-situ measurements for wavefront and polarization have been implemented.

The procedure for wavefront detection during the LIC test included the following steps: First, the irradiation with the 10 W fiber laser was blocked. Then the sample holder was translated by 5 millimetres to a calibration position. Then the shutter of the HeNe laser was opened and the wavefront sensors were calibrated (“plane wave calibration”). The sample holder was then moved back to its original position and the wavefront was measured. This way comparison of the transmitted wavefront on a pristine position on the optical sample to a position with a possible laser-induced deposit generated by the 1064 nm laser is obtained. This procedure means that there is only a short time (~30 seconds) between the calibration and the measurement with the wavefront sensors, which minimizes effects due to long-term sensor drifts or wavefront changes of the HeNe laser. For this procedure it is important that the HeNe laser does not generate LIC itself. This is ensured by using a short irradiation time (~15 seconds / wavefront measurement) and a low laser power density, as already mentioned. The described measurement procedure was performed automatically with a self-programmed software written in LabVIEW that controlled the laser beam shutters, the wavefront sensors and the translational stage of the sample holder.

4. RESULTS

4.1 Overview and in-situ test results

Table 2 provides an overview of the LIC tests described in this publication. Initially, we performed a bake-out of the vacuum chamber at temperatures up to 120°C and performed an LIC blank test with a laser fluence of 150 W/cm² to ensure the cleanliness of the chamber.

Table 2. Overview of LIC test parameters.

	Blank test	Test A	Test B	Test C	Test D
Temperature of contamination source/ °C	100	25	70	100	70
Laser fluence / (W/cm ²)	150	150	150	150	300
Irradiation time / hours	120	120	120	120	240
Mass loss of contaminant material mixture / mg	-	16.9	33.8	57.1	46.6
Mass loss of contaminant material mixture / %	-	0.34	0.73	1.13	0.93
Result of LIC test	Negative	Negative	Negative	Condensation	Negative

Subsequently, we performed a series of LIC tests with a fluence of 150 W/cm² and an increasing temperature of the contamination source to enhance the outgassing rate of the contaminant (Tests A, B and C). At the highest source temperature of 100 °C (Test C) we observed strong losses of transmission (tested for the AR coated optics) and reflection (tested for the HR coated optics), see Figure 6. From a microscopic inspection, this loss of transmission/reflection could clearly be attributed to a condensation of outgassing material on the front surface of the tested laser optics (see Figure 8). This is a result of the high temperature difference between the contamination source (100°C) and the laser optics under test 25°C.

In an attempt to accelerate the LIC test by other means, we have decided to perform another LIC test (Test D) with a temperature of 70°C and a higher laser fluence (300 W/cm²). Furthermore, the test duration was increased to 240 hours. Similar to LIC tests A and B, no deposit formation and no condensation was observed.

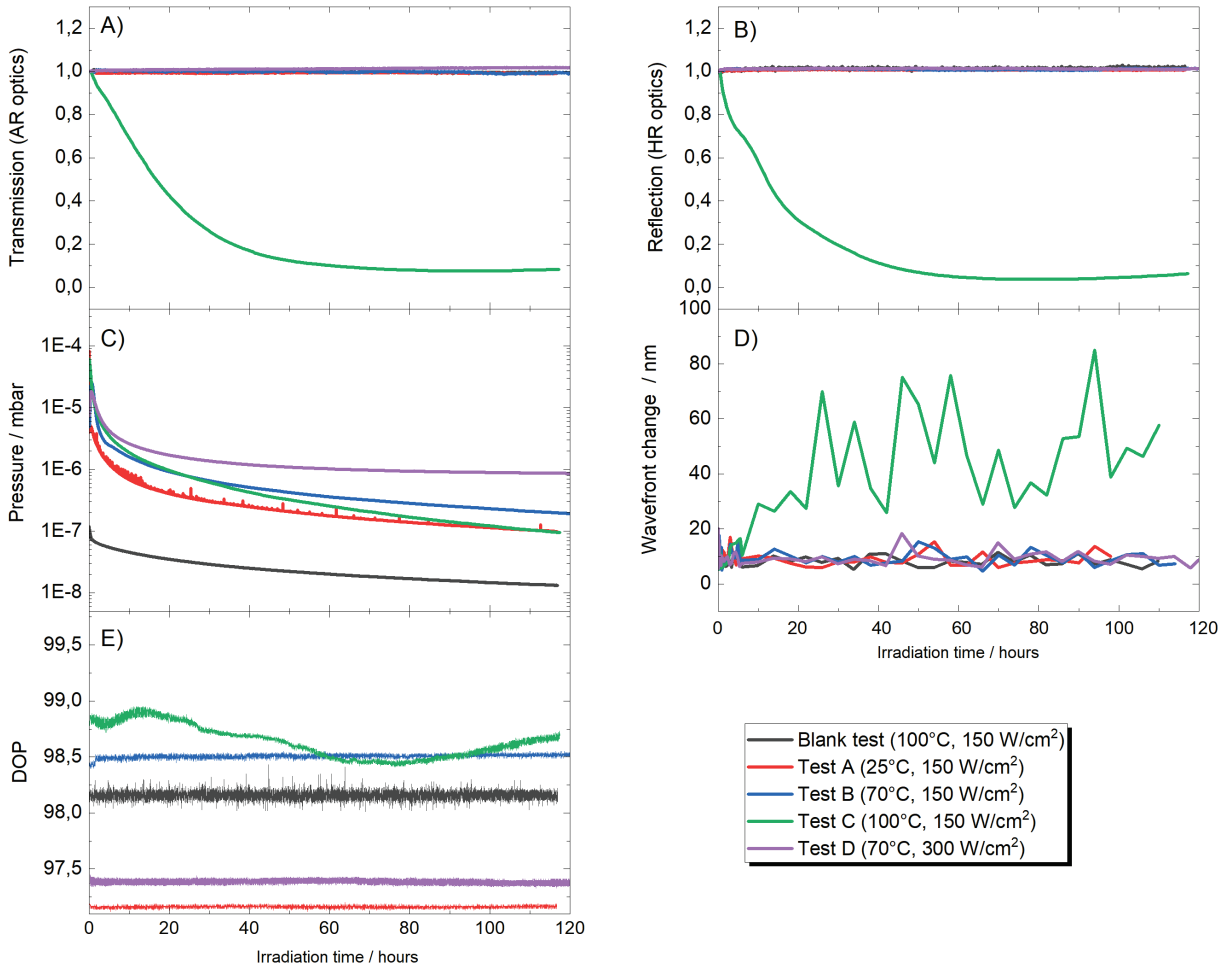


Figure 6: Results of in-situ measurements during the LIC tests. Panel A: Transmission of the anti-reflection coated optics. Panel B: Reflection of the high-reflection coated optics. Panel C: Pressure in the vacuum chamber as measured with an ion gauge. Panel D: Root-mean square (RMS) of the wavefront change as measured with Shack-Hartmann sensor B (with 4x beam expansion and a 150 μm MLA). Panel E: Degree of polarization measured in the beam reflected from the HR optics. Note that LIC Test D has continued until a total irradiation time of 240 hours without significant changes in the measured parameters (data not shown).

4.2 Changes in the transmitted wavefront due to condensation

The condensation observed in LIC test C also affected the wavefront of the transmitted laser beam, see Figure 7. Interestingly, this effect could only be observed with the Shack-Hartmann sensor B (with the higher lateral resolution). The change in wavefront was as high as ± 150 nm. The root-mean-square (RMS) of the wavefront change integrated over the detection area of the wavefront sensor is given in panel D of Figure 6 and increased up to ~ 60 nm. For the other LIC tests, the RMS of the wavefront change was below 10 nm.

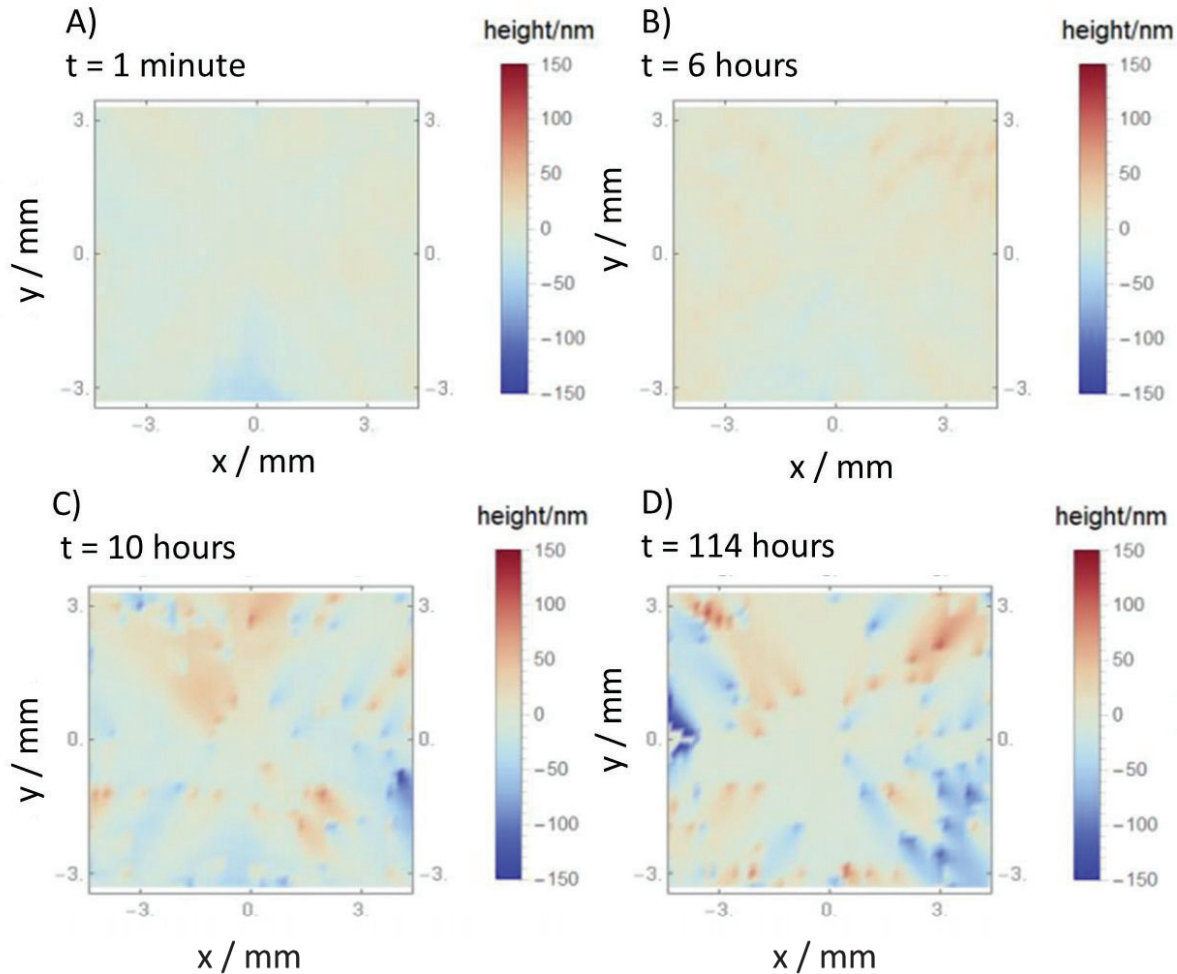


Figure 7: Change of wavefront during LIC Test D as measured with Shack-Hartmann sensor B. The changes in the wavefront are introduced by condensation of the front surface of the AR laser optics.

4.3 Microscopic inspection

All laser optics tested within this campaign have been analyzed with DIC and fluorescence microscopy at 2000x magnification. Except for the LIC test with condensation, we found no indication of a laser-induced deposit. From our experience, this means that no LIC with a height above ~ 5 nm was generated (detection limit).

Figure 8 shows a DIC micrograph of the front surface of the AR optics of LIC Test C showing the condensation products. The condensation occurs as droplets with a diameter of $\sim 10\mu\text{m}$. This is much smaller than the lateral resolution of the wavefront sensor even considering the 4 times beam expansion. This indicates that the wavefront change is introduced by inhomogeneities in the density of these droplets rather than due to an imaging of individual droplets.

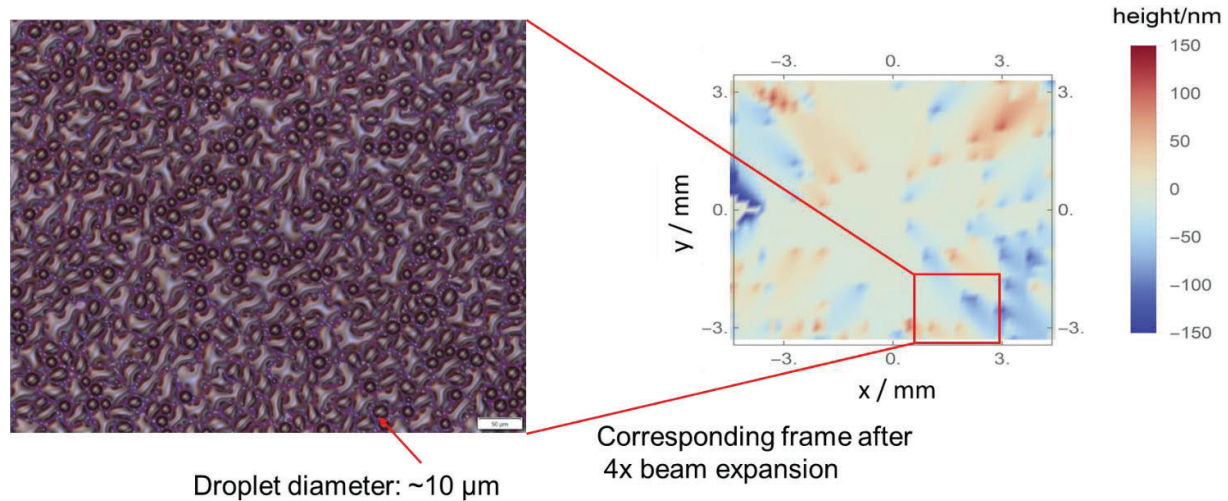


Figure 8: DIC micrograph of the AR optics (front surface) of Test C showing a strong condensation of outgassing material.

5. CONCLUSIONS & OUTLOOK

In order to assess the risk of LIC formation for the LISA mission, we have performed a series of LIC tests with mixture of 5 different contaminant materials and a laser-power density of up to 300 W/cm^2 . To accelerate LIC testing, the temperature of the contamination source was increased up to 100°C . At 100°C we observed condensation on the front surface of the optics under test kept at $\sim 25^\circ\text{C}$. Such a condensation is very unlikely to occur for the LISA mission, since the critical areas of the payload will be operating at a uniform temperature of only $(20 \pm 5)^\circ\text{C}$. Nonetheless, the laser might have parts with higher temperatures locally. During the design of the laser, we recommend to ensure that local temperatures above 70°C of potentially outgassing components are avoided.

For contaminant temperatures of up to 70°C , no LIC could be observed, neither with in-situ measurements nor via a microscopic inspection. This provides a lower limit of $\sim 5 \text{ nm}$ for a possible deposit formation. The reason that no LIC has been created is probably the rather low photon energy of the 1064 nm laser radiation (1.16 eV) compared to typical bond energies in organic molecules (e.g. 3.6 eV for a C-C chemical bond) in combination with the continuous wave operation of the laser, resulting in a low probability of multi-photon absorption compared to a pulsed laser operation. This is cautiously encouraging for the LISA mission.

However, only a limited set of potential materials has been screened up to now and for a limited test duration (5 days), which is short compared to the targeted mission lifetime. Given the draconian constraints on Wavefront Error (WFE) and long lifetime for LISA, it will nonetheless be necessary to take further risk assessment and mitigation measures.

We are currently performing long-duration LIC tests that will investigate a larger set of materials, featuring an improved LIC detection limit, over a test duration of up to 6 months to look for a possible deposit formation upon continued laser irradiation. This will give us a chance of better predicting the long-term behavior of LIC for the LISA mission. Furthermore, additional options for reducing risks of laser-induced contamination (e.g. the use of sealed compartments limiting the gas flow within the spacecraft) and options for additional testing during the assembly and integration phase of the LISA mission are being discussed.

REFERENCES

- [1] Gravitational Astrophysics Laboratory at NASA/GSFC, "<https://science.gsfc.nasa.gov/663/research/index.html>, 2022.
- [2] M. Hippler, P. Wagner, H. Schroeder and W. Riede, "Laser-induced contamination of space borne laser systems: impact of organic contamination and mitigation by oxygen," in *Systems Contamination: Prediction, Control, and Performance 2016*, 2016.
- [3] D. Kokkinos, H. Schroeder, K. Fleur-Frenette, M. P. Georges, W. Riede, G. Tzeremes and P. Rochus, "Laser optics in space failure risk due to laser induced contamination," *CEAS Space Journal*, vol. 9, pp. 153-162, 2017.
- [4] D. Wernham, J. Alves, F. Pettazzi and A. P. Tighe, "Laser-induced contamination mitigation on the ALADIN laser for ADM-Aeolus," in *Laser-Induced Damage in Optical Materials: 2010*, 2010.
- [5] H. Abdeldayem, E. Dowdye and J. Canham, "Roles of contamination and nonlinear effects in failing space-flight lasers," *Appl. Phys. B*, vol. 84, p. 447–452, 2006.
- [6] H. Schröder, P. Wagner, D. Kokkinos, W. Riede and A. Tighe, "Laser-induced contamination and its impact on laser damage threshold," in *Laser-Induced Damage in Optical Materials: 2013*, 2013.
- [7] F. E. Hovis, B. A. Shepherd, C. T. Radcliffe, A. L. Bailey and W. T. Boswell, "Optical damage at the part per million level: the role of trace contamination in laser-induced optical damage," in *Laser-Induced Damage in Optical Materials: 1993*, 1994.
- [8] N. Bartels, P. Allenspacher, T. Alig, I. Balasa, H. Schröder, G. Taube and W. Riede, "Laser-induced damage and contamination testing for the next generation of LIDAR space optics," in *International Conference on Space Optics — ICSO 2020*, 2021.
- [9] F. R. Wagner, G. G. E. Reaidy, D. Faye and J.-Y. Natoli, "Laser induced deposits in contaminated vacuum environment: Optical properties and lateral growth," *Optics & Laser Technology*, vol. 122, p. 105889, 2020.
- [10] P. L. Bender, "Wavefront distortion and beam pointing for LISA," *Classical and Quantum Gravity*, vol. 22, p. S339–S346, April 2005.
- [11] C. P. Sasso, G. Mana and S. Mottini, "Coupling of wavefront errors and jitter in the LISA interferometer: far-field propagation," *Classical and Quantum Gravity*, vol. 35, p. 185013, August 2018.
- [12] European Cooperation for Space Standardization, "ECSS-Q-ST-70-05C Rev.1: Detection of organic contamination surfaces by IR spectroscopy," 2019.
- [13] Spiricon Inc., "Hartmann Wavefront Analyzer Tutorial", "https://www.ophiropt.com/user_files/laser/beamprofilers/tutorial-hartman.pdf", 2004.
- [14] H. Schröder and W. Riede, "Laser damage lifetime tests under the presence of outgassing contaminants," *Final report for ESA contract 18633/04/NL/AR*, 2006.
- [15] Z. Hubka, J. Novák, I. Majerová, J. T. Green, P. K. Velpula, R. Boge, R. Antipenkov, V. Šobr, D. Kramer, K. Majer, J. A. Naylon, P. Bakule and B. Rus, "Mitigation of laser-induced contamination in vacuum in high-repetition-rate high-peak-power laser systems," *Appl. Opt.*, vol. 60, p. 533–538, January 2021.
- [16] I. T. Report, "Optics and photonics — Lasers and laser-related equipment — Laser-induced molecular contamination testing," *ISO/TR 20811:2017*, 2017.